

# A Generalized Computational Method to Determine Stability of a Multi-inverter Microgrid

Shivkumar V. Iyer, Madhu N. Belur, and Mukul C. Chandorkar, *Member, IEEE*

**Abstract**—Microgrid-containing parallel-connected inverters, where each inverter is controlled by decentralized active power/voltage frequency and reactive power/voltage magnitude droop control laws results in flexible and expandable systems. These systems have been known to have stability problems for large values of active power/voltage frequency droop control gain. However, so far the stability analysis of multi-inverter systems has always been performed in a computationally intensive manner by considering the entire microgrid. In a practical microgrid, where the number of inverters may be large or the capacity of the units may differ, it becomes essential to develop a method by which stability can be examined without much computational burden. The system of differential algebraic equations has been simplified using justifiable assumptions to result in a final expression that allows the stability of the microgrid to be examined separately with respect to the droop control laws of each inverter transformed into an equivalent network. Moreover, the procedure allows taking into consideration the  $R/X$  ratio of the interconnecting cables. Analysis of final expressions validate the stability results reported in literature. Experimental results on hardware show the stable operation of the microgrid.

**Index Terms**—Droop control laws, inverter, microgrid, model-order reduction, system modeling.

## I. INTRODUCTION

PARALLEL connection of inverters is an excellent strategy to build high-capacity reliable power supplies. A collection of loads and inverters fed by energy sources that can operate in isolation to the main ac grid is called a microgrid [1], [2]. Under the assumption that the energy sources feeding the inverters have sufficient capacity to supply the loads in the microgrid, an “intelligent” (centralized) control mechanism to manage balance of power generation and load demand is not necessary. Furthermore, a masterless control of inverters is desirable, where every inverter is a grid-forming unit defining the voltage frequency and magnitude of the microgrid. Under such circumstances, the failure of a given inverter does not cause a collapse of the microgrid and every inverter acts as a plug-and-play entity to make the

microgrid a conveniently expandable system. Communication links between the inverters or a supervisory controller are not essential for the stable operation of the microgrid, but can be used to enhance the transient performance of the microgrid.

The inverters in the microgrid are controlled by a nested control strategy. The inner controller ensures that the output voltage of the inverter tracks desired references [3]. The outer controller sets the references for the desired output voltages to be tracked by the inner controller. For a masterless control of the microgrid, the inverters are controlled to emulate synchronous generators in conventional power systems. The frequency and magnitude of the output voltages of an inverter varied with respect to the active power and reactive power supplied by the inverter, respectively [4]–[13]. This control strategy has been popularly termed as the droop control strategy and allows the inverters to share active and reactive power demanded by the loads in the microgrid according to their maximum rating. Moreover, the droop controller is a decentralized controller requiring only the measurements of variables local to the inverter. Stability issues of microgrids with inverters controlled by droop controllers has been widely reported in literature [10]–[13].

A complete eigenvalue analysis of the microgrid shows that the dominant eigenvalues are caused by the droop controller [10]–[13]. The voltage controller being implemented for fundamental and harmonic components has a high bandwidth. However, the droop controller requires measurement of active and reactive power supplied by the inverters that are either measured at low sampling rates or are filtered to obtain the low-frequency component [12], [13]. Therefore, the dominant eigenvalues of the microgrid can be examined by a detailed analysis of the droop controller. Published work has described how the system stability margin decreases with increase in the droop controller gains and the system finally becomes unstable for large values of active power/frequency droop gain [11]–[13]. Moreover, it has also been shown that the stability results are strongly dependent on the loading conditions of the microgrid and on network parameters.

The results already published are based on simulations of dynamical models of microgrids. These models are fairly dense and require a detailed knowledge of the system topology [11]–[13]. The prediction of stability is therefore a non-scalable analysis technique applicable only for microgrids not containing a large number of inverters. This paper proposes a reduced-order mathematical model of the microgrid in which the droop control laws acting on each inverter can be examined separately and the inverters are transformed into equivalent networks. From this mathematical model, the poles of the controlled system can be obtained. As shown by computation results in Scilab, the poles

Manuscript received December 14, 2009; revised February 4, 2010; accepted April 6, 2010. Date of current version September 17, 2010. Recommended for publication by Associate Editor J. M. Guerrero.

S. V. Iyer is with the Department of Electrical Engineering, Indian Institute of Technology Bombay, Mumbai, Maharashtra 400076, India, and also with ABB Global Industries and Services Ltd., Bengaluru 560048, India (e-mail: shivkiyer@yahoo.co.in).

M. N. Belur and M. C. Chandorkar are with the Department of Electrical Engineering, Indian Institute of Technology Bombay, Mumbai, Maharashtra 400076, India (e-mail: belur@ee.iitb.ac.in; mukul@ee.iitb.ac.in).

Digital Object Identifier 10.1109/TPEL.2010.2048720

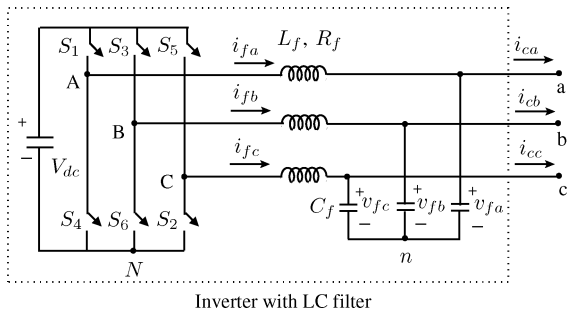


Fig. 1. Topology of the inverters.

of the controlled system obtained by the transfer functions are in close agreement with the results published. The poles and zeros of the open-loop plant have been plotted on the complex plane to predict instability with change in droop controller gains.

The outline of the paper is as follows. Section II describes the topology of the microgrid and the inverters. The mathematical model of the microgrid is written in the form of block matrices. Section III describes how the derived model is modified to decrease the size of the model being examined. Section IV derives the controller equations and their integration into the plant model derived in Section III to produce the controlled system model. The model of the controlled system is simplified using justifiable assumptions to present a closed-form expression through which the stability of the microgrid, with inverters controlled by droop control laws, can be systematically examined. Section V contains simulation results showing the stable boundaries of the microgrid and experimental results showing the stable operation of the microgrid. Section VI examines the sensitivity of the stable boundaries of the microgrid with respect to the  $R/X$  ratio of the interconnecting cables. Section VII concludes by highlighting the contributions of the paper and justifying the assumptions made.

## II. SYSTEM DESCRIPTION

This section describes the topology of the inverters, the topology of the microgrid chosen for study, and the derivation of the mathematical model of the microgrid. The system is a three-phase three-wire system and it is assumed that the network parameters are equal in all phases.

### A. Inverter Topology

Fig. 1 shows the topology of the three-phase three-wire inverter for interfacing a constant voltage source  $V_{dc}$  to the microgrid. The switches  $S_1$ – $S_6$  are insulated gate bipolar transistors (IGBTs) with their associated antiparallel diodes. The six IGBTs and the dc-voltage source form a voltage-source inverter (VSI), whose output is a switched waveform. The inductor  $L_f$  and the capacitor  $C_f$  form a low-pass  $L$ – $C$  filter that removes the high-frequency switching harmonics generated by the VSI. The voltages  $v_{fa}$ ,  $v_{fb}$ , and  $v_{fc}$  across the filter capacitor bank  $C_f$  are the output voltages of the inverter. The switches  $S_1$ – $S_6$  in Fig. 1 are switched by sine triangle pulsewidth modulation. Loh *et al.* [3] provided a detailed comparison of the different types

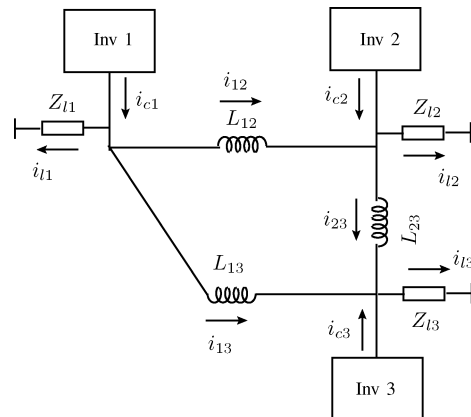


Fig. 2. Three-inverter-ring-connected microgrid.

of voltage controllers used for forcing the inverter to produce desired output voltages.

### B. Microgrid Topology

Fig. 2 is a single line diagram showing the topology of the three-phase microgrid used in the analysis. The microgrid is a three-inverter-ring-connected microgrid. In the blocks, “Inv” stands for inverter. Inverter 1, Inverter 2, and Inverter 3 have the topology of Fig. 1. Inverter 1, Inverter 2, and Inverter 3 have local loads  $Z_{l1}$ ,  $Z_{l2}$ , and  $Z_{l3}$  respectively. The loads have been assumed to be three-phase balanced linear passive loads consisting of resistances  $R_{l1}$ ,  $R_{l2}$ , and  $R_{l3}$  and inductances  $L_{l1}$ ,  $L_{l2}$ , and  $L_{l3}$ .  $L_{12}$ ,  $L_{23}$ , and  $L_{13}$  are the inductances of the cables connecting the inverters with associated resistances  $R_{12}$ ,  $R_{23}$ , and  $R_{13}$ , respectively.

### C. System Representation

In this section, mathematical model of the microgrid of Fig. 2 is developed; this is used for analysis. To simplify the process of system modeling, the microgrid is broken up into subsystems. The variables of each subsystem will be described later followed by the network laws that constrain the variables. Using Clarke’s transformation, the three-phase variables in the instantaneous reference frame will be transformed into variables in the synchronously rotating  $d$ – $q$  reference frame. The loads connected to the microgrid will be assumed to be balanced. As already stated, the network parameters in all three phases will be assumed to be equal. Therefore, under this assumption of a balanced three-phase system, the variables in the  $d$ – $q$  reference frame will be constant dc quantities in steady state. To reduce the number of variables and constraining equations, all the transformed variables that have  $d$  and  $q$  components will be expressed as complex variables with a real  $d$  part and an imaginary  $q$  part. The analysis will be performed in the small signal sense with the variables expressed as deviations of values from an equilibrium point. Furthermore, a Laplace transformation is performed on the system assuming the initial conditions to be zero.

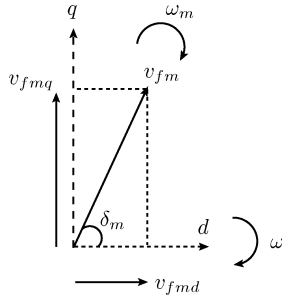


Fig. 3. Complex variable  $v_{fm}$  and its projections  $v_{fmd}$  and  $v_{fmq}$ .

The complex variables of the microgrid will be collected together to form a vector  $\mathbf{x}$ . Furthermore, variables are grouped in a suitable manner to form subvectors within  $\mathbf{x}$  that will result in a mathematical model that possesses a convenient block matrix structure. The vector containing all the variables of the microgrid is

$$\mathbf{x} = (\mathbf{u}, \mathbf{x}_v, \mathbf{x}_c, \mathbf{x}_\ell, \mathbf{x}_{\text{int}}). \quad (1)$$

The subvectors are as follows:

$$\begin{aligned} \mathbf{u} &= (u_1, u_2, u_3) \\ \mathbf{x}_v &= (v_{f1}, v_{f2}, v_{f3}) \\ \mathbf{x}_c &= (i_{c1}, i_{c2}, i_{c3}) \\ \mathbf{x}_\ell &= (i_{\ell1}, i_{\ell2}, i_{\ell3}) \\ \mathbf{x}_{\text{int}} &= (i_{12}, i_{23}, i_{13}). \end{aligned} \quad (2)$$

In the aforementioned equations, the variables in the vectors are complex. For example,  $v_{f1} = v_{f1d} + jv_{f1q}$ ,  $i_{c1} = i_{c1d} + ji_{c1q}$ ,  $i_{\ell1} = i_{\ell1d} + ji_{\ell1q}$ , and  $i_{12} = i_{12d} + ji_{12q}$ . The complex variable  $u_1$  is the input to Inverter 1 and is defined as  $u_1 = \delta_1 - jV_1$ . Other variables  $u_2$  and  $u_3$  can be written in a similar manner with appropriate changes in the subscripts. The laws constraining these variables will be described next.

The variable  $u_m = \delta_m - jV_m$  for inverter  $m$  ( $m = 1, 2, 3$ ) is derived with respect to Fig. 3. With respect to Fig. 3, the angle  $\delta_m$  is written as follows [10]:

$$\delta_m = \tan^{-1} \left( \frac{v_{fmq}}{v_{fmd}} \right).$$

The aforementioned equation is a nonlinear equation and is therefore linearized about the equilibrium point and expressed in the small signal sense

$$\Delta\delta_m = -\frac{V_{fmq}}{V_{fmd}^2 + V_{fmq}^2} \Delta v_{fmd} + \frac{V_{fmd}}{V_{fmd}^2 + V_{fmq}^2} \Delta v_{fmq}. \quad (3)$$

In (3),  $V_{fmd}$  and  $V_{fmq}$  are the values of the variables  $v_{fmd}$  and  $v_{fmq}$ , respectively, at the equilibrium point. The variable  $V_m$  that denotes the magnitude of the inverter output voltage is defined as follows:

$$V_m = \sqrt{\frac{v_{fmd}^2 + v_{fmq}^2}{V_{fmd}^2 + V_{fmq}^2}}.$$

The aforementioned nonlinear equation is linearized to

$$\Delta V_m = \frac{V_{fmd}}{V_{fmd}^2 + V_{fmq}^2} \Delta v_{fmd} + \frac{V_{fmq}}{V_{fmd}^2 + V_{fmq}^2} \Delta v_{fmq}. \quad (4)$$

The complex variable  $u_m = \delta_m - jV_m$  is therefore defined in the small signal sense as follows:

$$\Delta u_m = k_{um} \Delta v_{fm} = \frac{-V_{fmq} - jV_{fmd}}{V_{fmd}^2 + V_{fmq}^2} \Delta v_{fm}. \quad (5)$$

The aforementioned equation can be extended to all three inverters and written as a matrix equation as follows:

$$[-\mathbf{A}_u \quad \mathbf{I}] \begin{bmatrix} \Delta \mathbf{u} \\ \Delta \mathbf{x}_v \end{bmatrix} = 0 \quad (6)$$

where

$$\mathbf{A}_u = \begin{bmatrix} \frac{1}{k_{u1}} & 0 & 0 \\ 0 & \frac{1}{k_{u2}} & 0 \\ 0 & 0 & \frac{1}{k_{u3}} \end{bmatrix}.$$

The load laws at the three inverters form the next set of equations. As an example, the load law at Inverter 1 is written in the small signal sense as follows:

$$\Delta v_{f1} - Z_{\ell1} \Delta i_{\ell1} = 0$$

where  $Z_{\ell m} = R_{\ell m} + sL_{\ell m} + j\omega L_{\ell m}$  for  $m = 1, 2, 3$ . The load laws can be combined into one single matrix equation as follows:

$$[-\mathbf{A}_\ell \quad \mathbf{I}] \begin{bmatrix} \Delta \mathbf{x}_v \\ \Delta \mathbf{x}_\ell \end{bmatrix} = 0 \quad (7)$$

where

$$\mathbf{A}_\ell = \begin{bmatrix} \frac{1}{Z_{\ell1}} & 0 & 0 \\ 0 & \frac{1}{Z_{\ell2}} & 0 \\ 0 & 0 & \frac{1}{Z_{\ell3}} \end{bmatrix}.$$

The KCL laws describing the relationship between the inverter output current and the currents through interconnecting cables connected to the inverters are written as follows:

$$\begin{aligned} \Delta i_{c1} - \Delta i_{\ell1} - \Delta i_{12} - \Delta i_{13} &= 0 \\ \Delta i_{c2} - \Delta i_{\ell2} + \Delta i_{12} - \Delta i_{23} &= 0 \\ \Delta i_{c3} - \Delta i_{\ell3} + \Delta i_{23} + \Delta i_{13} &= 0. \end{aligned} \quad (8)$$

The aforementioned laws can be written in the matrix form as follows:

$$[\mathbf{I} \quad -\mathbf{I} \quad \mathbf{A}_{\text{int}}] \begin{bmatrix} \Delta \mathbf{x}_c \\ \Delta \mathbf{x}_\ell \\ \Delta \mathbf{x}_{\text{int}} \end{bmatrix} = 0 \quad (9)$$

where

$$\mathbf{A}_{\text{int}} = \begin{bmatrix} -1 & 0 & -1 \\ 1 & -1 & 0 \\ 0 & 1 & 1 \end{bmatrix}.$$

The interaction between inverters through the impedance of the interconnecting cables are described by KVL laws written as follows:

$$\begin{aligned} \Delta v_{f1} - \Delta v_{f2} - Z_{12} \Delta i_{12} &= 0 \\ \Delta v_{f2} - \Delta v_{f3} - Z_{23} \Delta i_{23} &= 0 \\ \Delta v_{f1} - \Delta v_{f3} - Z_{13} \Delta i_{13} &= 0 \end{aligned} \quad (10)$$

where, as an example,  $Z_{12} = R_{12} + sL_{12} + j\omega L_{12}$ . The aforementioned laws can be written in the matrix form as follows:

$$[-\mathbf{A}_z \quad \mathbf{I}] \begin{bmatrix} \Delta \mathbf{x}_v \\ \Delta \mathbf{x}_{\text{int}} \end{bmatrix} = 0 \quad (11)$$

where

$$\mathbf{A}_z = \begin{bmatrix} \frac{1}{Z_{12}} & -\frac{1}{Z_{12}} & 0 \\ 0 & \frac{1}{Z_{23}} & -\frac{1}{Z_{23}} \\ \frac{1}{Z_{13}} & 0 & -\frac{1}{Z_{13}} \end{bmatrix}.$$

The complete model of the microgrid in terms of the block matrices is as follows:

$$\begin{aligned} \mathbf{A}_{\text{total}} \Delta \mathbf{x} &= 0 \quad (12) \\ \begin{bmatrix} -\mathbf{A}_u & \mathbf{I} & 0 & 0 & 0 \\ 0 & 0 & \mathbf{I} & -\mathbf{I} & \mathbf{A}_{\text{int}} \\ 0 & -\mathbf{A}_\ell & 0 & \mathbf{I} & 0 \\ 0 & -\mathbf{A}_z & 0 & 0 & \mathbf{I} \end{bmatrix} \begin{bmatrix} \Delta \mathbf{u} \\ \Delta \mathbf{x}_v \\ \Delta \mathbf{x}_c \\ \Delta \mathbf{x}_\ell \\ \Delta \mathbf{x}_{\text{int}} \end{bmatrix} &= 0. \quad (13) \end{aligned}$$

### III. PLANT MODEL REDUCTION

In Section II, the open-loop plant model of the microgrid had been derived and presented in a block matrix manner. However, the model did not include the droop control strategy. In order to examine the stability of the closed-loop microgrid with the droop controller, the droop controller equations will be appended to the plant model. The characteristic polynomial of the controlled system will be the determinant of the complete model containing the plant equations and the controller equations. However, if the closed-loop characteristic polynomial is obtained by computing the determinant of the matrix obtained by merely appending the controller equations to the plant model, the computational burden required turns out to be significant. Therefore, the plant model will be manipulated and reduced to a convenient form that allows stability to be examined with lesser computational burden.

The plant model is seen to act on the vector  $\Delta \mathbf{x}$  that contains all the variables of the microgrid. However, the droop controller is a decentralized controller that acts on variables local to the inverters. The objective of simplification will therefore be to eliminate the variables that do not affect the droop controller. Fig. 4 show the input–output division of the variables in the plant model. Fig. 5 shows the droop controllers implemented for Inverter 1, Inverter 2, and Inverter 3. As can be seen from Fig. 5, only the output voltage  $v_f$  of an inverter and the output

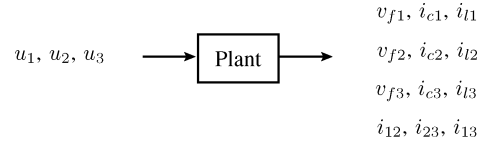


Fig. 4. Input–output division of variables.

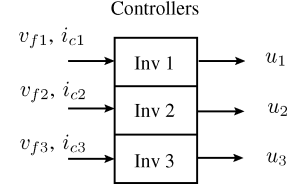


Fig. 5. Implementation of droop controllers.

current  $i_c$  are measured for implementing the droop controller for that particular inverter.

The method of simplifying the plant mathematical model is along the following principles. A unimodular matrix is a square matrix, whose determinant is a nonzero constant. Premultiplication of a matrix  $\mathbf{A}$  by a unimodular matrix  $\mathbf{U}$  when studying the set of solutions to  $\mathbf{A}w = 0$  is equivalent to performing elementary row operations on the matrix. However, such elementary row operations will not change the solution set of the matrix equations. Moreover, the determinant of the resultant matrix  $\mathbf{U}\mathbf{A}$  is the product of the determinant of the unimodular matrix and determinant of the original matrix. Therefore, since the determinant of the unimodular matrix is a nonzero constant, the determinant of the resultant matrix produces the characteristic polynomial of the controlled system. The characteristic polynomial of a system is the polynomial, whose roots are the poles of the system, counted with multiplicity.

The unimodular matrix, which has been chosen as a premultiplier to the plant model matrix developed in the previous section, is written as follows:

$$\mathbf{U} = \begin{bmatrix} \mathbf{I} & 0 & 0 & 0 \\ \mathbf{A}_\ell - \mathbf{A}_{\text{int}} \mathbf{A}_z & \mathbf{I} & \mathbf{I} & -\mathbf{A}_{\text{int}} \\ 0 & 0 & \mathbf{I} & 0 \\ 0 & 0 & 0 & \mathbf{I} \end{bmatrix}. \quad (14)$$

It is to be noted that  $\det(\mathbf{U}) = 1$ . The resultant matrix obtained is written as follows:

$$\mathbf{U}\mathbf{A}_{\text{total}} = \begin{bmatrix} -\mathbf{A}_u & \mathbf{I} & 0 & 0 & 0 \\ -(\mathbf{A}_\ell - \mathbf{A}_{\text{int}} \mathbf{A}_z) \mathbf{A}_u & 0 & \mathbf{I} & 0 & 0 \\ 0 & -\mathbf{A}_\ell & 0 & \mathbf{I} & 0 \\ 0 & -\mathbf{A}_z & 0 & 0 & \mathbf{I} \end{bmatrix}. \quad (15)$$

As already stated, the decentralized droop controller that is applied to every inverter requires the measurement of variables local to the concerned inverter. These variables are the output voltage  $v_f$  and the output current  $i_c$ . The controller equations will be derived in the next section. However, the structure of the controller along with the structure of the plant model will

be utilized to reduce the order of the plant model that is being analyzed.

The decentralized droop controller is written in the following block matrix form:

$$\mathbf{C} = [\mathbf{C}_{\text{inp}} \quad \mathbf{C}_{vf} \quad \mathbf{C}_{ic} \quad 0 \quad 0]. \quad (16)$$

The controlled system or the closed-loop system consists of the controller matrix equations appended with the plant model equations. The controlled system is written as follows:

$$\mathbf{A}_{\text{micro}} \Delta \mathbf{x} = 0 \quad (17)$$

where

$$\mathbf{A}_{\text{micro}} = \begin{bmatrix} -\mathbf{A}_u & \mathbf{I} & 0 & 0 & 0 \\ -(\mathbf{A}_\ell - \mathbf{A}_{\text{int}} \mathbf{A}_z) \mathbf{A}_u & 0 & \mathbf{I} & 0 & 0 \\ \mathbf{C}_{\text{inp}} & \mathbf{C}_{vf} & \mathbf{C}_{ic} & 0 & 0 \\ \hline 0 & -\mathbf{A}_\ell & 0 & \mathbf{I} & 0 \\ 0 & -\mathbf{A}_z & 0 & 0 & \mathbf{I} \end{bmatrix}. \quad (18)$$

The aforementioned matrix has been written in a block structure that will be used in simplifying the determinant computation, as shown.

The computation of the determinant of  $\mathbf{A}_{\text{micro}}$  provides the characteristic polynomial of the controlled system from which its stability can be analyzed. The Schur's complement result can be utilized to compute the determinant of  $\mathbf{A}_{\text{micro}}$  as follows. Consider any matrix  $\mathbf{R}$  written in the block diagonal form

$$\mathbf{R} = \begin{bmatrix} \mathbf{R}_{11} & \mathbf{R}_{12} \\ \mathbf{R}_{21} & \mathbf{R}_{22} \end{bmatrix}.$$

Using Schur's complement, the determinant of the matrix  $\mathbf{R}$  is written as follows:

$$|\mathbf{R}| = |\mathbf{R}_{11} + \mathbf{R}_{12} \mathbf{R}_{22}^{-1} \mathbf{R}_{21}| |\mathbf{R}_{22}|. \quad (19)$$

The Schur's complement as defined here requires that the matrix  $\mathbf{R}_{22}$  is invertible. From the block diagonal representation of  $\mathbf{A}_{\text{micro}}$ , it can be observed that Schur's complement is applicable due to the presence of the identity matrix in place of  $\mathbf{R}_{22}$ . Moreover, since  $\mathbf{R}_{12}$  is zero, the determinant of  $\mathbf{A}_{\text{micro}}$  reduces to

$$|\mathbf{A}_{\text{micro}}| = \begin{vmatrix} -\mathbf{A}_u & \mathbf{I} & 0 \\ -(\mathbf{A}_\ell - \mathbf{A}_{\text{int}} \mathbf{A}_z) \mathbf{A}_u & 0 & \mathbf{I} \\ \mathbf{C}_{\text{inp}} & \mathbf{C}_{vf} & \mathbf{C}_{ic} \end{vmatrix}. \quad (20)$$

The block matrix  $\mathbf{A}_\ell - \mathbf{A}_{\text{int}} \mathbf{A}_z$  happens to have a systematic structure.

$$\mathbf{A}_\ell - \mathbf{A}_{\text{int}} \mathbf{A}_z = \begin{bmatrix} \frac{1}{Z_{\ell 1}} + \frac{1}{Z_{12}} + \frac{1}{Z_{13}} & -\frac{1}{Z_{12}} & -\frac{1}{Z_{13}} \\ -\frac{1}{Z_{12}} & \frac{1}{Z_{\ell 2}} + \frac{1}{Z_{12}} + \frac{1}{Z_{23}} & -\frac{1}{Z_{23}} \\ -\frac{1}{Z_{13}} & -\frac{1}{Z_{23}} & \frac{1}{Z_{\ell 2}} + \frac{1}{Z_{13}} + \frac{1}{Z_{23}} \end{bmatrix}. \quad (21)$$

In general, for any microgrid with inverters connected together by cables, the aforementioned equations can be written in a similar manner. The diagonal elements are the sum of terms

corresponding to the load connected at the inverter and the admittances of the cables connecting the inverter to other inverters. The off-diagonal element  $mn$  is the negative of the admittance of the cable between inverter  $m$  and inverter  $n$  when inverter  $m$  and inverter  $n$  are connected. In the case of inverter  $m$  not being connected to inverter  $n$ , the off-diagonal term  $mn$  will be zero. A further approximation can be made is that  $|Z_l| \gg |Z_{\text{cable}}|$ , since the cable impedances are essentially parasitic. Therefore, the admittances corresponding to the load impedances  $Z_{l1}$ ,  $Z_{l2}$ , and  $Z_{l3}$  are neglected and dropped from further expressions.

#### IV. CONTROLLER EQUATIONS

The droop controllers applied to every inverter varies the voltage frequency and voltage magnitude from their nominal values as linear functions of the active and reactive power supplied by the inverter, respectively. Mathematically, the droop controller equations for inverter  $m$  are written as follows [4]–[13]:

$$\begin{aligned} \omega_m &= s\delta_m = \omega_0 - k_{pm} p_m \\ V_m &= V_0 - k_{qm} q_m \end{aligned} \quad (22)$$

where  $\omega_0$  and  $V_0$  are the nominal values of angular frequency and voltage magnitude, respectively. They have been chosen to be  $100\pi$  rad/s and 230 V, respectively. The angular frequency  $\omega_m$  of inverter  $m$  output voltage has been expressed as a derivative of the phase angle  $\delta_m$  derived earlier.  $k_{pm}$  and  $k_{qm}$  are the droop coefficients, while  $p_m$  and  $q_m$  are the active power and reactive power supplied by the inverter, respectively. The first equation is called the  $p$ - $\omega$  droop control law, while the second equation is called the  $q$ - $V$  droop law.

The active power and reactive power supplied by the inverter are written as follows:

$$\begin{aligned} p_m &= v_{fmd} i_{cmd} + v_{fmq} i_{cmq} \\ q_m &= v_{fmq} i_{cmd} - v_{fmd} i_{cmq}. \end{aligned}$$

It is to be noted that the aforementioned equations contain the  $d$  and  $q$  components of variables as real separate variables. Moreover, the aforementioned equations are seen to have a product nonlinearity, and therefore, are linearized about the equilibrium point as follows:

$$\begin{aligned} \Delta p_m &= I_{cmd} \Delta v_{fmd} + I_{cmq} \Delta v_{fmq} + V_{fmd} \Delta i_{cmd} \\ &\quad + V_{fmq} \Delta i_{cmq} \\ \Delta q_m &= -I_{cmq} \Delta v_{fmd} + I_{cmd} \Delta v_{fmq} + V_{fmq} \Delta i_{cmd} \\ &\quad - V_{fmd} \Delta i_{cmq} \end{aligned}$$

where  $I_{cmd}$  and  $I_{cmq}$  are the values of the output currents  $i_{cmd}$  and  $i_{cmq}$  of inverter  $m$ , respectively, at the equilibrium point.

Linearizing the droop controller equations, and substituting the expressions for  $\Delta p_m$  and  $\Delta q_m$ , the following expressions are obtained:

$$\begin{aligned} s\Delta\delta_m &= -k_{pm} (I_{cmd} \Delta v_{fmd} + I_{cmq} \Delta v_{fmq} + V_{fmd} \Delta i_{cmd} \\ &\quad + V_{fmq} \Delta i_{cmq}) \end{aligned}$$

$$\Delta V_m = k_{qm}(I_{cmq}\Delta v_{fmd} - I_{cmd}\Delta v_{fmq} - V_{fmq}\Delta i_{cmd} + V_{fmd}\Delta i_{cmq}). \quad (23)$$

The droop controller equations for the three inverter units in the microgrid are written in the matrix form as follows:

$$\begin{bmatrix} s\mathbf{I} \\ 0 \end{bmatrix} \Delta \delta + \begin{bmatrix} 0 \\ \mathbf{I} \end{bmatrix} \Delta \mathbf{V} + \begin{bmatrix} \mathbf{C}_{vd} \\ \mathbf{D}_{vd} \end{bmatrix} \Delta \mathbf{x}_{vd} + \begin{bmatrix} \mathbf{C}_{vq} \\ \mathbf{D}_{vq} \end{bmatrix} \Delta \mathbf{x}_{vq} + \begin{bmatrix} \mathbf{C}_{id} \\ \mathbf{D}_{id} \end{bmatrix} \Delta \mathbf{x}_{cd} + \begin{bmatrix} \mathbf{C}_{iq} \\ \mathbf{D}_{iq} \end{bmatrix} \Delta \mathbf{x}_{cq} = 0. \quad (24)$$

The vectors in the aforementioned equation are the real, and imaginary vectors corresponding to the complex vectors of (2) are as follows:

$$\begin{aligned} \delta &= [\delta_1 \quad \delta_2 \quad \delta_3] \\ \mathbf{V} &= [-V_1 \quad -V_2 \quad -V_3] \\ \mathbf{x}_{vd} &= [v_{f1d} \quad v_{f2d} \quad v_{f3d}] \\ \mathbf{x}_{vq} &= [v_{f1q} \quad v_{f2q} \quad v_{f3q}] \\ \mathbf{x}_{cd} &= [i_{c1d} \quad i_{c2d} \quad i_{c3d}] \\ \mathbf{x}_{cq} &= [i_{c1q} \quad i_{c2q} \quad i_{c3q}]. \end{aligned}$$

The reason for choosing  $\mathbf{V}$  with negative signs in the voltage magnitudes is to remain in compliance with the definition of  $u = \delta - jV$ . The following vectors are also defined:

$$\begin{aligned} \mathbf{k}_p &= [k_{p1} \quad k_{p2} \quad k_{p3}] \\ \mathbf{k}_q &= [k_{q1} \quad k_{q2} \quad k_{q3}]. \end{aligned}$$

The matrices are as follows:

$$\mathbf{C}_{vd} = \begin{bmatrix} k_{p1}I_{c1d} & 0 & 0 \\ 0 & k_{p2}I_{c2d} & 0 \\ 0 & 0 & k_{p3}I_{c3d} \end{bmatrix}.$$

The aforementioned matrix is written as a product of diagonal matrices as follows:

$$\mathbf{C}_{vd} = [\text{diag}(\mathbf{k}_p) \times \text{diag}(\mathbf{X}_{cd})]$$

where  $\text{diag}(\mathbf{k}_p)$  implies a diagonal matrix, whose diagonal elements are the vector  $\mathbf{k}_p$  and  $\mathbf{X}_{cd}$  is the values of the vector  $\mathbf{x}_{cd}$  at the equilibrium point. Similarly

$$\begin{aligned} \mathbf{C}_{vq} &= [\text{diag}(\mathbf{k}_p) \times \text{diag}(\mathbf{X}_{cq})] \\ \mathbf{C}_{id} &= [\text{diag}(\mathbf{k}_p) \times \text{diag}(\mathbf{X}_{vd})] \\ \mathbf{C}_{iq} &= [\text{diag}(\mathbf{k}_p) \times \text{diag}(\mathbf{X}_{vq})] \\ \mathbf{D}_{vd} &= [\text{diag}(\mathbf{k}_q) \times \text{diag}(\mathbf{X}_{cd})] \\ \mathbf{D}_{vq} &= [-\text{diag}(\mathbf{k}_q) \times \text{diag}(\mathbf{X}_{cd})] \\ \mathbf{D}_{id} &= [-\text{diag}(\mathbf{k}_q) \times \text{diag}(\mathbf{X}_{vq})] \\ \mathbf{D}_{iq} &= [\text{diag}(\mathbf{k}_q) \times \text{diag}(\mathbf{X}_{vd})]. \end{aligned}$$

In the previous section, the plant model was derived using complex variables. The following vector is defined:

$$\mathbf{x}_{cld} = [\delta \quad \mathbf{V} \quad \mathbf{x}_{vd} \quad \mathbf{x}_{vq} \quad \mathbf{x}_{cd} \quad \mathbf{x}_{cq}].$$

However, as shown earlier, the controller utilizes the real components of the complex variables. As a result, the plant model derived will be modified so as to act on the real variables. Rewriting the matrix  $\mathbf{A}_{red}$  such that it acts on real variables

$$\mathbf{A}_{cld} \Delta \mathbf{x}_{cld} = 0 \quad (25)$$

$$\begin{bmatrix} -\mathbf{A}_u^r & \mathbf{A}_u^i & \mathbf{I} & 0 & 0 & 0 \\ -\mathbf{A}_u^i & -\mathbf{A}_u^r & 0 & \mathbf{I} & 0 & 0 \\ -\mathbf{A}_{imp}^r & \mathbf{A}_{imp}^i & 0 & 0 & \mathbf{I} & 0 \\ -\mathbf{A}_{imp}^i & -\mathbf{A}_{imp}^r & 0 & 0 & 0 & \mathbf{I} \\ s\mathbf{I} & 0 & \mathbf{C}_{vd} & \mathbf{C}_{vq} & \mathbf{C}_{id} & \mathbf{C}_{iq} \\ 0 & \mathbf{I} & \mathbf{D}_{vd} & \mathbf{D}_{vq} & \mathbf{D}_{id} & \mathbf{D}_{iq} \end{bmatrix} \begin{bmatrix} \Delta \delta \\ \Delta \mathbf{V} \\ \Delta \mathbf{x}_{vd} \\ \Delta \mathbf{x}_{vq} \\ \Delta \mathbf{x}_{cd} \\ \Delta \mathbf{x}_{cq} \end{bmatrix} = 0 \quad (26)$$

where  $\mathbf{A}_{imp} = (\mathbf{A}_\ell - \mathbf{A}_{int} \mathbf{A}_z) \mathbf{A}_u$ .  $\mathbf{A}_u^r$  and  $\mathbf{A}_u^i$  are the real and imaginary components of the matrix  $\mathbf{A}_u$  while  $\mathbf{A}_{imp}^r$  and  $\mathbf{A}_{imp}^i$  are the real and imaginary components of the matrix  $\mathbf{A}_{imp}$ . The determinant of the matrix  $\mathbf{A}_{cld}$  in the aforementioned equation provides the characteristic polynomial. In a manner similar to obtain the reduced-order plant model, the matrix  $\mathbf{A}_{cld}$  in the aforementioned equation will also be reduced, as described later.

The matrix  $\mathbf{A}_{cld}$  will be premultiplied by a unimodular matrix (described in Section III, paragraph 3). The unimodular matrix is chosen to be

$$\mathbf{U}_{cld} = \begin{bmatrix} \mathbf{I} & 0 & 0 & 0 & 0 & 0 \\ 0 & \mathbf{I} & 0 & 0 & 0 & 0 \\ 0 & 0 & \mathbf{I} & 0 & 0 & 0 \\ 0 & 0 & 0 & \mathbf{I} & 0 & 0 \\ -\mathbf{C}_{vd} & -\mathbf{C}_{vq} & -\mathbf{C}_{id} & -\mathbf{C}_{iq} & \mathbf{I} & 0 \\ -\mathbf{D}_{vd} & -\mathbf{D}_{vq} & -\mathbf{D}_{id} & -\mathbf{D}_{iq} & 0 & \mathbf{I} \end{bmatrix}. \quad (27)$$

It is to be noted that  $\det(\mathbf{U}) = 1$ . The matrix product  $\mathbf{U}_{cld} \mathbf{A}_{cld}$  is

$$\mathbf{U}_{cld} \mathbf{A}_{cld} = \begin{bmatrix} -\mathbf{A}_u^r & \mathbf{A}_u^i & \mathbf{I} & 0 & 0 & 0 \\ -\mathbf{A}_u^i & -\mathbf{A}_u^r & 0 & \mathbf{I} & 0 & 0 \\ -\mathbf{A}_{imp}^r & \mathbf{A}_{imp}^i & 0 & 0 & \mathbf{I} & 0 \\ -\mathbf{A}_{imp}^i & -\mathbf{A}_{imp}^r & 0 & 0 & 0 & \mathbf{I} \\ \hline \mathbf{C}_\delta^{\text{mod}} & \mathbf{C}_V^{\text{mod}} & 0 & 0 & 0 & 0 \\ \mathbf{D}_\delta^{\text{mod}} & \mathbf{D}_V^{\text{mod}} & 0 & 0 & 0 & 0 \end{bmatrix}. \quad (28)$$

Following the similar arguments for reducing the matrix  $\mathbf{A}_{micro}$ , the determinant of the matrix  $\mathbf{A}_{cld}$  is written using the Schur's complement as follows:

$$|\mathbf{A}_{cld}| = \begin{vmatrix} \mathbf{C}_\delta^{\text{mod}} & \mathbf{C}_V^{\text{mod}} \\ \mathbf{D}_\delta^{\text{mod}} & \mathbf{D}_V^{\text{mod}} \end{vmatrix}. \quad (29)$$

The matrices  $\mathbf{C}_\delta^{\text{mod}}$ ,  $\mathbf{C}_V^{\text{mod}}$ ,  $\mathbf{D}_\delta^{\text{mod}}$ , and  $\mathbf{D}_V^{\text{mod}}$  are written as follows:

$$\mathbf{C}_\delta^{\text{mod}} = s\mathbf{I} + \mathbf{C}_{vd} \mathbf{A}_u^r + \mathbf{C}_{vq} \mathbf{A}_u^i + \mathbf{C}_{id} \mathbf{A}_{imp}^r + \mathbf{C}_{iq} \mathbf{A}_{imp}^i \quad (30)$$

$$\mathbf{C}_V^{\text{mod}} = -\mathbf{C}_{vd} \mathbf{A}_u^i + \mathbf{C}_{vq} \mathbf{A}_u^r - \mathbf{C}_{id} \mathbf{A}_{imp}^i + \mathbf{C}_{iq} \mathbf{A}_{imp}^r \quad (31)$$

$$\mathbf{D}_\delta^{\text{mod}} = \mathbf{D}_{vd}\mathbf{A}_u^r + \mathbf{D}_{vq}\mathbf{A}_u^i + \mathbf{D}_{id}\mathbf{A}_{\text{imp}}^r + \mathbf{D}_{iq}\mathbf{A}_{\text{imp}}^i \quad (32)$$

$$\mathbf{D}_V^{\text{mod}} = \mathbf{I} - \mathbf{D}_{vd}\mathbf{A}_u^i + \mathbf{D}_{vq}\mathbf{A}_u^r - \mathbf{D}_{id}\mathbf{A}_{\text{imp}}^i + \mathbf{D}_{iq}\mathbf{A}_{\text{imp}}^r. \quad (33)$$

The aforementioned equations appear to be complicated and each of the matrices  $\mathbf{C}_\delta^{\text{mod}}$ ,  $\mathbf{C}_V^{\text{mod}}$ ,  $\mathbf{D}_\delta^{\text{mod}}$ , and  $\mathbf{D}_V^{\text{mod}}$  have elements that contain several terms. However, by making an approximation that will be described next, many of the terms will be found to cancel out leaving matrices that have a convenient structure.

The droop controller allows inverters to share active and reactive power demanded by the loads in the microgrid by varying the frequency and magnitude of the output voltages of the inverters. Active power flow across a predominantly inductive cable is closely coupled to the phase angle difference between the voltages at the two ends of the cable [4]. Similarly, the reactive power flow is closely coupled to the difference in magnitudes of the voltages at the two ends of the cable when the cable is predominantly inductive [4]. The assumption of all cables being predominantly inductive is followed in the paper so that the droop control strategy is effective in power sharing between the inverters.

By changing the frequency during transients, a difference in phase angle across a cable between two inverters is produced that allows control of active power flow. Similarly, by changing magnitudes of the output voltages of the inverter, a voltage magnitude difference is produced across cables that results in reactive power flow control. The following assumptions are therefore made.

- 1) The phase angle difference would depend on the impedances of the cables connecting the inverters for a certain active power flowing across the cable. These impedances can be assumed to be very small, and therefore, the phase angle differences between the inverters will also be small.
- 2) Similarly, the difference in the magnitudes of the output voltages of the inverters will be very small.
- 3) The output voltages of the inverters can be considered to be very close in phase and magnitude. Therefore, at the chosen equilibrium point, the  $d$  and  $q$  components of all the inverter output voltages are assumed to be approximately equal. For this microgrid,  $V_{f1d} \approx V_{f2d} \approx V_{f3d} =: V_{fd}$  and  $V_{f1q} \approx V_{f2q} \approx V_{f3q} =: V_{fq}$ .

With the aforementioned approximations, the matrices  $\mathbf{C}_\delta^{\text{mod}}$ ,  $\mathbf{C}_V^{\text{mod}}$ ,  $\mathbf{D}_\delta^{\text{mod}}$ , and  $\mathbf{D}_V^{\text{mod}}$  simplify to

$$\mathbf{C}_\delta^{\text{mod}} = s\mathbf{I} + \text{diag}(\mathbf{k}_p) [-\mathbf{Q} + (V_{fd}^2 + V_{fq}^2)\mathbf{X}] \quad (34)$$

$$\mathbf{Q} = \text{diag}(Q_1, Q_2, Q_3)$$

$$\mathbf{X} = \begin{bmatrix} X_{12} + X_{13} & -X_{12} & -X_{13} \\ -X_{12} & X_{12} + X_{23} & -X_{23} \\ -X_{13} & -X_{23} & X_{13} + X_{23} \end{bmatrix}$$

where  $X_{mn} = \omega L_{mn}/|Z_{mn}|^2$  and  $|Z_{mn}|^2 = (R_{mn} + sL_{mn})^2 + (\omega L_{mn})^2$  have been substituted due to space constraints

$$\mathbf{C}_V^{\text{mod}} = \text{diag}(\mathbf{k}_p) [-\mathbf{P} - (V_{fd}^2 + V_{fq}^2)\mathbf{Y}] \quad (35)$$

$$\mathbf{P} = \text{diag}(P_1, P_2, P_3)$$

$$\mathbf{Y} = \begin{bmatrix} Y_{12} + Y_{13} & -Y_{12} & -Y_{13} \\ -Y_{12} & Y_{12} + Y_{23} & -Y_{23} \\ -Y_{13} & -Y_{23} & Y_{13} + Y_{23} \end{bmatrix}$$

where  $Y_{mn} = (R_{mn} + sL_{mn})/|Z_{mn}|^2$  has been substituted due to space constraints

$$\mathbf{D}_\delta^{\text{mod}} = \text{diag}(\mathbf{k}_q) [-\mathbf{P} + (V_{fd}^2 + V_{fq}^2)\mathbf{Y}] \quad (36)$$

$$\mathbf{D}_V^{\text{mod}} = \mathbf{I} + \text{diag}(\mathbf{k}_q) [\mathbf{Q} + (V_{fd}^2 + V_{fq}^2)\mathbf{X}]. \quad (37)$$

The aforementioned matrices have a very convenient structure similar to the structure of  $\mathbf{A}_\ell - \mathbf{A}_{\text{int}}\mathbf{A}_z$ . Moreover, as earlier stated, such a structure will be obtained for any microgrid with inverters connected together by cables. The matrices can be written by mere inspection of the microgrid topology. A few comments are to be made regarding these matrices.  $P_m$  and  $Q_m$  are the active and reactive power supplied by inverter  $m$  at the equilibrium point, respectively. The variable  $\omega$  in the matrices is the value of the angular frequency of the microgrid at equilibrium when the frequencies of all inverter units are equal. With the  $p$ - $\omega$  droops producing a drop in frequency of the order of 1% to 2%,  $\omega \approx \omega_0$ . Similarly,  $(V_{fd}^2 + V_{fq}^2)$  is merely equal to the square of the voltage magnitude of the voltage vectors. The  $q$ - $V$  droop produces a drop in the voltage magnitudes of the order of 2% to 4%. Therefore,  $(V_{fd}^2 + V_{fq}^2) \approx V_0^2$ . When the system is represented in the per unit system, both  $\omega_0$  and  $V_0$  will be equal to 1.

The matrices in the aforementioned equations are completely comprised of the inductances and resistances of the interconnecting cables and the active and reactive powers supplied by inverter units at the equilibrium point. The determinant  $|\mathbf{A}_{\text{cld}}|$  will be a polynomial depending on the elements of  $\mathbf{C}_\delta^{\text{mod}}$ ,  $\mathbf{C}_V^{\text{mod}}$ ,  $\mathbf{D}_\delta^{\text{mod}}$ , and  $\mathbf{D}_V^{\text{mod}}$ . A simplification will be described next to neglect the higher order terms of droop control gains in the polynomial.

From (34)–(37), it is evident that the determinant of the matrix  $\mathbf{A}_{\text{cld}}^{\text{mod}}$  has off-diagonal terms that are multiplied by the control gains  $k_{p1}$ ,  $k_{p2}$ , and  $k_{p3}$  and  $k_{q1}$ ,  $k_{q2}$ , and  $k_{q3}$ . The diagonal terms on the other hand are polynomials that contain the control gains. The determinant of such a matrix can be described using an example as follows. The determinant of an  $n \times n$  matrix  $\mathbf{B}$  is written as follows:

$$\mathbf{B} = \sum_{\sigma \in S_n} \text{sgn}(\sigma) \prod_{m=1}^n b_{m,\sigma(m)}. \quad (38)$$

In (38), the sum is computed over all permutations  $\sigma$  of the ordered set  $\{1, 2, \dots, n\}$ . The  $\text{sgn}(\sigma)$  is a sign function associated with a permutation. The ordered set  $\{1, 2, \dots, n\}$  provides the first permutation. Therefore, the first term is the product  $b_{1\sigma(1)}b_{2\sigma(2)} \dots b_{n\sigma(n)}$ , which is the product of the diagonal terms  $b_{11}b_{22} \dots b_{nn}$ . Consider a term where a permutation has been made such that  $\sigma(r) = s$  for any  $r \neq s$  in the ordered set  $\{1, 2, \dots, n\}$ . Therefore, the product will not contain the terms  $b_{rr}$  and  $b_{ss}$ , but will contain off-diagonal terms in their place. The product of two off-diagonal terms will result in a product of two droop control gains.

Using a  $3 \times 3$  matrix, an illustration can be made

$$\mathbf{B} = \begin{bmatrix} s + k_{p1}b_{11} & k_{p1}b_{12} & k_{p1}b_{13} \\ k_{p2}b_{21} & s + k_{p2}b_{22} & k_{p2}b_{23} \\ k_{p3}b_{31} & k_{p3}b_{32} & s + k_{p3}b_{33} \end{bmatrix}.$$

The determinant of the aforementioned matrix will contain six products corresponding to  $3!$  permutations. The determinant is written as follows:

$$\begin{aligned} |\mathbf{B}| &= (s + k_{p1}b_{11})(s + k_{p2}b_{22})(s + k_{p3}b_{33}) \\ &\quad - k_{p2}k_{p3}b_{23}b_{32}(s + k_{p1}b_{11}) - k_{p1}k_{p2}b_{12}b_{21}(s + k_{p3}b_{33}) \\ &\quad - k_{p1}k_{p3}b_{13}b_{31}(s + k_{p2}b_{22}) + k_{p1}k_{p2}k_{p3}b_{12}b_{23}b_{31} \\ &\quad + k_{p1}k_{p2}k_{p3}b_{13}b_{21}b_{32}. \end{aligned} \quad (39)$$

The first term in the determinant is the product of the diagonal terms. The second, third, and fourth terms are seen to be terms multiplied by a product of two droop control gains. The fifth and sixth terms are seen to be terms multiplied by a product of three droop control gains. The droop control gains  $k_p$  and  $k_q$  are usually very small so that the drop in voltage frequency and voltage magnitude will be within an acceptable range of their nominal values. Therefore, a product of two or more droop control gains will result in a term that is negligible. Therefore,  $|\mathbf{B}|$  can be approximated to

$$|\mathbf{B}| \approx (s + k_{p1}b_{11})(s + k_{p2}b_{22})(s + k_{p3}b_{33}). \quad (40)$$

Similarly, the determinant of the  $\mathbf{A}_{cld}$  can be approximated to the product of the diagonal terms alone and is written as follows:

$$\begin{aligned} |\mathbf{A}_{cld}| &= \left[ s + k_{p1} \left( -Q_1 + \frac{\omega L_{12}}{|Z_{12}|^2} + \frac{\omega L_{13}}{|Z_{13}|^2} \right) \right] \\ &\quad \left[ s + k_{p2} \left( -Q_2 + \frac{\omega L_{12}}{|Z_{12}|^2} + \frac{\omega L_{23}}{|Z_{23}|^2} \right) \right] \\ &\quad \times \left[ s + k_{p3} \left( -Q_3 + \frac{\omega L_{13}}{|Z_{13}|^2} + \frac{\omega L_{23}}{|Z_{23}|^2} \right) \right] \\ &\quad \left[ 1 + k_{q1} \left( Q_1 + \frac{\omega L_{12}}{|Z_{12}|^2} + \frac{\omega L_{13}}{|Z_{13}|^2} \right) \right] \\ &\quad \times \left[ 1 + k_{q2} \left( Q_2 + \frac{\omega L_{12}}{|Z_{12}|^2} + \frac{\omega L_{23}}{|Z_{23}|^2} \right) \right] \\ &\quad \left[ 1 + k_{q3} \left( Q_3 + \frac{\omega L_{13}}{|Z_{13}|^2} + \frac{\omega L_{23}}{|Z_{23}|^2} \right) \right]. \end{aligned} \quad (41)$$

In general, for any inverter  $m$  in the microgrid, the following two polynomials are written:

$$\begin{aligned} s + k_{pm} \left( -Q_m + \sum_{\{n\}} \frac{\omega L_{mn}}{|Z_{mn}|^2} \right) \\ 1 + k_{qm} \left( Q_m + \sum_{\{n\}} \frac{\omega L_{mn}}{|Z_{mn}|^2} \right) \end{aligned} \quad (42)$$

where  $\{n\}$  is the set of all inverters to which inverter  $m$  is connected. As can be seen from the aforementioned equations, each inverter in the microgrid appears to be transformed into an

equivalent network with the interconnecting impedances connecting it to other inverters taken into account. The droop control laws are then applied to this equivalent network providing two polynomials for each inverter. Therefore, the properties of the controlled system can be examined by examining each polynomial with a single droop coefficient individually. The roots of the aforementioned polynomial when written for each inverter provide the poles of the controlled system. The computational burden of evaluating a single polynomial is far lesser than the computation of the determinant of the entire system model, as has been reported in literature. As an example, one polynomial is evaluated next.

Consider the first polynomial in the product

$$s + k_{p1} \left( -Q_1 + \frac{\omega L_{12}}{|Z_{12}|^2} + \frac{\omega L_{13}}{|Z_{13}|^2} \right) = 0. \quad (43)$$

This can be simplified to

$$\begin{aligned} s|Z_{12}|^2|Z_{13}|^2 + k_{p1}(-Q_1|Z_{12}|^2|Z_{13}|^2 + \omega L_{12}|Z_{13}|^2 \\ + \omega L_{13}|Z_{12}|^2) = 0. \end{aligned}$$

The aforementioned equation is in the standard root locus form of  $\text{den}(s) + k \text{num}(s) = 0$ , where  $k = k_{p1}$  is the control gain and  $\text{num}(s)/\text{den}(s)$  is the plant transfer function. Furthermore, the roots of  $\text{num}(s)$  and  $\text{den}(s)$  provide the zeros and poles of the open-loop plant, respectively, using which the root loci and stability of the system for change in control gains can be predicted. The poles and zeros of the plant transfer functions correspond to closed-loop poles for  $k \rightarrow 0$  and  $k \rightarrow \infty$ , respectively. They can be computed as roots of  $sZ_{12}^2Z_{13}^2$  and  $-Q_1Z_{12}^2Z_{13}^2 + \omega L_{12}Z_{13}^2 + \omega L_{13}Z_{12}^2$ . We use Scilab to compute the roots and plot them in the complex  $s$  plane.

## V. SIMULATION AND EXPERIMENTAL RESULTS

Section V-A shows through simulations in Scilab, the movement of poles of the controlled system for variation in the control gains. Section V-B shows experimental results from a hardware setup of a three-inverter-ring-connected microgrid. The experimental results show the stable operation of the microgrid with desired power sharing between the inverters.

### A. Simulation Results

A three-inverter-ring-connected microgrid of Fig. 2 is considered for study. The simulation results presented in this section examines the stability of the controlled system having the characteristic polynomial of (41). Equation (41) contains the following.

- 1) The impedances  $Z_{12}$ ,  $Z_{23}$ , and  $Z_{13}$  of the cables.
- 2) The active and reactive power supplied by each inverter at the equilibrium point about which the system is linearized.
- 3) The  $p$ - $\omega$  droop control gains  $k_{p1}$ ,  $k_{p2}$ , and  $k_{p3}$  and the  $q$ - $V$  droop control gains  $k_{q1}$ ,  $k_{q2}$ , and  $k_{q3}$ .

The simulations are performed with the system parameters in per unit. The parameters of the base system are listed in Table I.

TABLE I  
BASE SYSTEM PARAMETERS

Base VA = 5000, Base Voltage = 400 V
Base Current = 6.95 A, Base frequency = 50 Hz
Base Impedance = 34.44Ω, Base Inductance = 0.109 H

The impedances of the cables have been chosen for the simulation study as follows:

$$R_{12} = 0.01 \Omega, L_{12} = 150 \mu\text{H}$$

$$R_{23} = 0.01 \Omega, L_{23} = 200 \mu\text{H}$$

$$R_{13} = 0.01 \Omega, L_{13} = 250 \mu\text{H}.$$

The cables have been chosen with low  $R/X$  ratio for the droop laws of (22) to be effective. The inductances of the cables has been chosen to be different. The droop control gains of the inverters are chosen to be equal, i.e,  $k_{p1} = k_{p2} = k_{p3}$  and  $k_{q1} = k_{q2} = k_{q3}$ . Since the  $p$ - $\omega$  and  $q$ - $V$  droop control gains of the inverters are equal, the inverters are assumed to supply equal active and reactive power at the equilibrium point, which are  $P_1 = P_2 = P_3 = 3450 \text{ W}$  and  $Q_1 = Q_2 = Q_3 = 4500 \text{ VAR}$ .

The stability of the microgrid is analyzed by plotting the roots of the six polynomials in the determinant of the controlled system of (41). This equation shows that the stability of the controlled system is decided by the stability of the constituent polynomials. The determinant of the controlled system is rewritten naming the constituent polynomials

$$|\mathbf{A}_{clid}| = a_{p\omega 1}(s)a_{p\omega 2}(s)a_{p\omega 3}(s) \times a_{qV 1}(s)a_{qV 2}(s)a_{qV 3}(s). \quad (44)$$

The polynomials  $a_{p\omega 1}(s)$ ,  $a_{p\omega 2}(s)$ , and  $a_{p\omega 3}(s)$  contain the gains  $k_{p1}$ ,  $k_{p2}$ , and  $k_{p3}$ , respectively. The polynomials  $a_{qV 1}(s)$ ,  $a_{qV 2}(s)$ , and  $a_{qV 3}(s)$  contain the gains  $k_{q1}$ ,  $k_{q2}$ , and  $k_{q3}$ , respectively. The roots of these polynomials change with variations in their droop control gains. Furthermore, using Scilab or MATLAB, the exact values of the control gains that cause instability will be obtained.

As described in the previous section, each polynomial can be written in the form of  $\text{den}(s) + k \text{ num}(s) = 0$  with  $\text{num}(s)/\text{den}(s)$  resembling a plant transfer function. Table II lists the zeros of the transfer function that are the roots of  $\text{num}(s)$  and the poles that are the roots of  $\text{den}(s)$ . When the roots of the polynomials are plotted for varying positive gains, as per theory of root locus plots, the loci originate from the poles of the transfer function for zero gain and terminate at the zeros as gain tends to infinity. In the figures given next, the zeros of the transfer function are plotted as ‘‘o,’’ while the poles are plotted at ‘‘x.’’ However, as can be seen from Table II, some of the zeros are far away from the dominant poles. While plotting these zeros, they are scaled and brought closer to the dominant poles to improve the clarity of the plots.

Fig. 6(a)–(c) shows the movement of the roots of the polynomials  $a_{p\omega 1}(s)$ ,  $a_{p\omega 2}(s)$ , and  $a_{p\omega 3}(s)$  as their respective control gains  $k_{p1}$ ,  $k_{p2}$ , and  $k_{p3}$  are varied. The arrows indicate the direction of movement of the roots as the control gain increases. The

TABLE II  
ZEROS AND POLES OF THE POLYNOMIALS

Polynomial	Zeros (p.u)	Poles (p.u)
$a_{p\omega 1}(s)$	$-0.16 \pm j$ 34.3 $-34.7$	$-0.13 \pm j$ $-0.21 \pm j$ 0
$a_{p\omega 2}(s)$	$-0.18 \pm j$ 36.1 $-36.5$	$-0.15 \pm j$ $-0.21 \pm j$ 0
$a_{p\omega 3}(s)$	$-0.14 \pm j$ 31.7 $-36.5$	$-0.12 \pm j$ $-0.16 \pm j$ 0
$a_{qV 1}(s)$	$-0.16 \pm j$ $-0.18 \pm j$ 34.3	$-0.13 \pm j$ $-0.21 \pm j$
$a_{qV 2}(s)$	$-0.18 \pm j$ $-0.19 \pm j$ 36.1	$-0.15 \pm j$ $-0.21 \pm j$
$a_{qV 3}(s)$	$-0.14 \pm j$ $-0.14 \pm j$ 31.7	$-0.12 \pm j$ $-0.16 \pm j$

plots are very similar in some aspects. In all the plots, the roots move into the right half of the  $s$  plane for large values of the control gain. As the roots are the poles of the controlled system, this indicates instability for large values of control gain. The zeros are scaled and plotted closer to the imaginary axis to improve the clarity of the plot. Therefore, the zero on the right half of the  $s$  plane implies that the controlled system is unstable for large gains with root loci moving closer toward it. The value of the control gains  $k_{p1}$ ,  $k_{p2}$ , and  $k_{p3}$  for which the controlled system becomes unstable is found through Scilab to be 0.0051 p.u. or  $3.21 \times 10^{-4} \text{ rad/(Ws)}$ . The value of  $k_{p1}$ ,  $k_{p2}$ , and  $k_{p3}$  at which the microgrid became unstable are equal in this case because the microgrid considered is small containing only three inverters and the values of the impedances of the cables connecting them are very close. For larger microgrids, instability will result at distinct values of the  $p$ - $\omega$  droop control gain.

Fig. 7(a)–(c) are plots of the poles (marked by ‘‘x’’) of  $a_{qV 1}(s)$ ,  $a_{qV 2}(s)$ , and  $a_{qV 3}(s)$  with respect to  $k_{q1}$ ,  $k_{q2}$ , and  $k_{q3}$ , respectively. The ‘‘o’’ indicates the zeros of the transfer function. However, it is to be noted that the zero has been scaled and plotted closer to the real axis in order to improve the clarity of the plot. As before, the arrows indicate the direction of movement of the roots of the polynomials as the control gains increase. As can be seen from the plot, the controlled system does not lose stability as the  $q$ - $V$  droop control gains vary.

## B. Experimental Results

This section provides experimental results to prove the stable operation of the microgrid when the inverters are controlled by the droop control laws. The experiments are conducted on a low-voltage level three-phase microgrid of 140 V. The inverters are formed of commercial inverters of the three-leg single dc capacitor topology shown in Fig. 1. The dc capacitor of the inverters are charged through single-phase rectifiers to maintain a dc voltage of 300 V. The inductor–capacitor ( $L_f$ – $C_f$ ) filter connected at the output of the inverter, as shown in Fig. 1, has the parameters  $L_f = 3 \text{ mH}$  and  $C_f = 200 \mu\text{F}$ . Each inverter has its own associated control board containing the

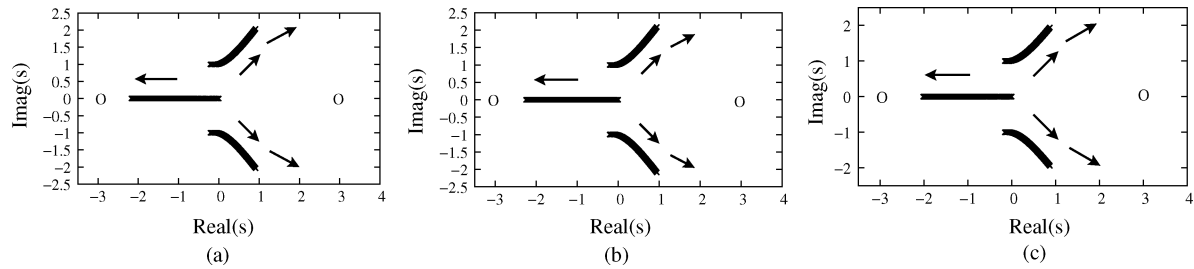


Fig. 6. Variation of roots of  $a_{p\omega 1}(s)$ ,  $a_{p\omega 2}(s)$ , and  $a_{p\omega 3}(s)$  for variation of  $k_{p1}$ ,  $k_{p2}$ , and  $k_{p3}$ , respectively. (a) Roots of  $a_{p\omega 1}(s)$ . (b) Roots of  $a_{p\omega 2}(s)$ . (c) Roots of  $a_{p\omega 3}(s)$ .

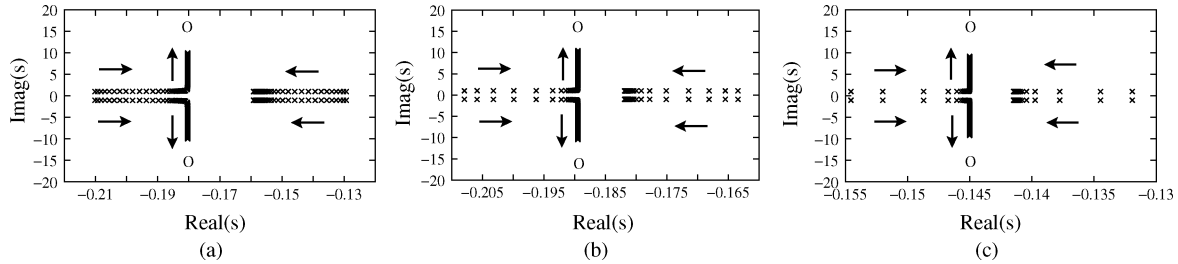


Fig. 7. Variation of roots of  $a_{qV 1}(s)$ ,  $a_{qV 2}(s)$ , and  $a_{qV 3}(s)$  for variation of  $k_{q1}$ ,  $k_{q2}$ , and  $k_{q3}$ , respectively. (a) Roots of  $a_{qV 1}(s)$ . (b) Roots of  $a_{qV 2}(s)$ . (c) Roots of  $a_{qV 3}(s)$ .

Texas Instruments TMS320VC33 floating point processor. The voltages and currents required for control are measured by a sensing circuit, converted into analog signals between 0 and 5 V, and fed to a 12-bit analog-to-digital converter AD7864. The control laws are implemented in the DSP and control the switching of the inverters. The droop control gains for the inverters are chosen as  $k_{p1} = k_{p2} = k_{p3} = 0.0125$  rad/(Ws) and  $k_{q1} = k_{q2} = k_{q3} = 0.005$  V/VAR.

Fig. 8 shows the operation of the inverters when they are not connected in parallel to form a microgrid, but operating in the stand-alone mode. The output voltages of the inverters can be seen to be relatively smooth sinusoids having a magnitude close to 85 V, which results in a line-to-line voltage of 140 V. The output currents of the inverters are seen to be unequal due to unequal local load connected at the inverters. The local load connected at Inverter 1 consists of six 250 V, 200 W incandescent lamps and a three-phase reactor bank of 0.012 H per phase. The local load connected at Inverter 2 consists of four 250 V, 200 W incandescent lamps, while local load at Inverter 3 consists of six 250 V, 200 W incandescent lamps. Therefore, the output current of Inverter 1 is far greater than the output currents of Inverter 2 and Inverter 3.

Fig. 9 shows the phase  $a$  output voltages of the inverters when connected in parallel to form a microgrid. The voltages are seen to have magnitudes that are approximately equal and are almost in phase with each other. This is due to the fact that the interconnecting impedances being of the order 150 – 200  $\mu$ H, very small phase angle differences or the voltage magnitude differences are required for the inverters to share load power demand equally. Fig. 10 shows the phase  $a$  output currents of the inverters when forming the microgrid. The currents supplied by the inverters indicate a roughly equal power sharing between the inverters.

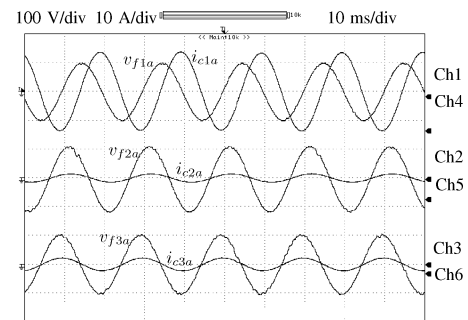


Fig. 8. Inverters' phase  $a$  output voltages and currents in stand-alone operation.

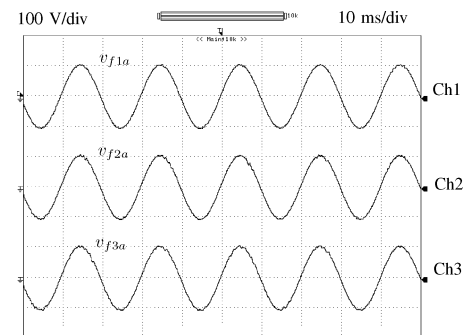


Fig. 9. Phase  $a$  output voltages of the inverters when forming the microgrid.

Fig. 11 shows the active and reactive power supplied by the inverters when connected in parallel to form the microgrid. Fig. 11(a) shows that the active power supplied by the inverters are equal since they have  $p$ - $\omega$  droop control gains that are equal  $k_{p1} = k_{p2} = k_{p3}$ . Fig. 11(b) shows the reactive power supplied by the inverters to be unequal despite the  $q$ - $V$  droop control gains being equal  $k_{q1} = k_{q2} = k_{q3}$ . The unequal sharing of

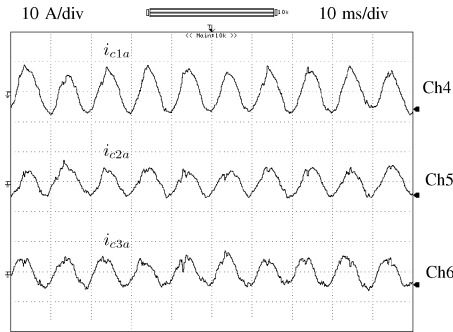


Fig. 10. Phase  $a$  output currents of the inverters when forming the microgrid.

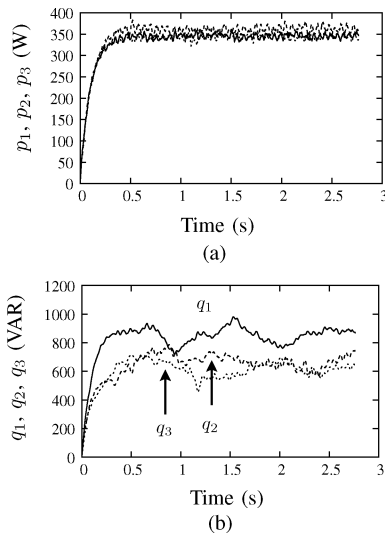


Fig. 11. Active and reactive power supplied by the inverters. (a) Active power supplied by the inverters. (b) Reactive power supplied by the inverters. (c) Active and reactive power supplied by the inverters.

reactive power is due to the fact that the voltage magnitudes of the inverters are also constrained by network laws besides the  $q$ - $V$  droop laws. As a result of which, reactive power is not shared in exactly the manner as desired. Since, the reactive power demand of the load at Inverter 1 is the highest, Inverter 1 continues to supply the largest fraction of the load demand.

Furthermore, both the plots, but particularly the reactive power flow plot, contain significant low-order harmonics. This is due to the damped low-frequency oscillations produced by the dominant poles of the controlled system lying close to the imaginary axis. These low-frequency oscillations decrease in magnitude as time progresses. These low-frequency oscillations are also reported in literature [12].

## VI. SENSITIVITY TO $R/X$ RATIO

In this section, the applicability of the results for a broader class of microgrids will be discussed. The  $R/X$  ratio of the interconnecting cables play an important role in the stability margin of the microgrid. This section will examine the effect of variation of  $R/X$  ratio of the interconnecting cables.

The variation of the eigenvalues of the controlled system with respect to system parameters are observed through the

roots of the polynomials of (41). As an example, the roots of the polynomials containing the  $p$ - $\omega$  droop gain and  $q$ - $V$  droop gain of Inverter 1 will be examined as follows:

$$\left[ s + k_{p1} \left( -Q_1 + \frac{\omega L_{12}}{|Z_{12}|^2} + \frac{\omega L_{13}}{|Z_{13}|^2} \right) \right] \left[ 1 + k_{q1} \left( Q_1 + \frac{\omega L_{12}}{|Z_{12}|^2} + \frac{\omega L_{13}}{|Z_{13}|^2} \right) \right] = 0. \quad (45)$$

After rearranging, (45) can be expressed in standard root loci forms as the transfer functions of equivalent plants in cascade as follows:

$$\left[ d_{p\omega 1} + k_{p1} n_{p\omega 1} \right] \left[ d_{qV 1} + k_{q1} n_{qV 1} \right] = 0 \quad (46)$$

where  $d_{p\omega 1} = s|Z_{12}|^2|Z_{13}|^2$  and  $d_{qV 1} = |Z_{12}|^2|Z_{13}|^2$  resemble the denominators of the transfer function of the equivalent plants of (45). The numerators of the equivalent plant  $n_{p\omega 1}$  and  $n_{qV 1}$  can be written from (45). However, for reasons that will be described later, the focus will be on the open-loop poles obtained from the denominators  $d_{p\omega 1}$  and  $d_{qV 1}$ . From  $d_{p\omega 1} = 0$  and  $d_{qV 1} = 0$ , the open-loop poles of the equivalent plant are as follows:

$$\begin{aligned} \text{Poles}_{p\omega 1} &= 0, -\frac{R_{12}}{L_{12}} \pm j\omega, -\frac{R_{13}}{L_{13}} \pm j\omega \\ \text{Poles}_{qV 1} &= -\frac{R_{12}}{L_{12}} \pm j\omega, -\frac{R_{13}}{L_{13}} \pm j\omega \end{aligned} \quad (47)$$

As can be seen from the aforementioned expressions, the open-loop poles of the equivalent transformed system are strongly influenced by the ratio of the resistance to inductance ( $R/L$ ) of the interconnecting cables. By considering a nominal angular frequency, the  $R/L$  ratio can be interpreted as the  $R/X$  ratio that is available for cables through data sheets. As this ratio of  $R/X$  increases, the open-loop poles move further into the left half of the complex  $s$  plane. In a similar manner, the  $R/X$  ratio and the impedance  $Z_{mn}$  of the cable between Inverter  $m$  and Inverter  $n$  will affect the open-loop zeros of the equivalent plant. This evident from (45).

However, while plotting the root locus of the transfer function of the equivalent plant, the root loci will originate from the open-loop poles at zero gains, i.e.,  $k_{p1} = 0$  and  $k_{q1} = 0$  and terminate at the open-loop zeros when the droop control gains tend to infinity, i.e.,  $k_{p1} \rightarrow \infty$  and  $k_{q1} \rightarrow \infty$ . As already stated, the droop control gains are chosen to be small to ensure that the voltage frequency and voltage magnitude are within limits. Typically,  $k_{p1}$  will be in the range of 1%–2% and  $k_{q1}$  will be within 2%–4%. Therefore, the relevant part of the root locus for the droop control strategy is in the vicinity of the open-loop poles. As observed from the aforementioned equation, the stability margin of the controlled system will increase for increasing  $R/X$  ratio of the interconnecting cables due to the open-loop poles of the equivalent plant moving into the left half of the complex  $s$  plane.

## VII. CONCLUSION

The stability of multi-inverter microgrids has been examined with respect to a three-inverter-ring-connected microgrid. As

has been reported in literature, the interconnections between the inverters and the choice of droop control gains play a significant role in the stability of the microgrid. The model of the microgrid that has been derived in this paper considers only the effect of the droop control gains and the topology of the microgrid. The voltage controller associated with each inverter that ensures the inverters to produce desired output voltages has not been included in the model. The voltage controller has been shown to have a high bandwidth, thereby resulting in dynamics that are significantly faster than the droop control dynamics [12], [13]. However, even without the voltage controller, the mathematical model of a three-inverter microgrid is considerably complex. Literature contains stability analysis of microgrid by examining the complete mathematical model. However, analysis based on complete models are difficult for microgrids with a large number of inverters and complex interconnections due to the computational burden.

The significant contribution in this paper has been to simplify the mathematical model using justifiable assumptions to a form that can be examined with reduced computational burden, from which the stable boundaries of the microgrid are determined accurately. It has been shown that the stability of the microgrid can be analyzed with each inverter transformed into an equivalent network. The impedances of the interconnections play a significant role and are included in each equivalent inverter network by mere knowledge of the connectivity of the concerned inverter to other inverters. The effect of the droop control laws can be examined separately. This is under the assumption that the interconnection cables are predominantly inductive and the droop laws can be decoupled. The model for a large and complex microgrid can therefore be written as a product of models of each inverter with its droop control laws. The computational burden required to analyze the stability of these individual models is significantly lower.

The proof of stability in Sections II–IV that result in the generalized equation of (42) has been based on several assumptions. The assumptions will be summarized next with a brief justification of their validity for microgrids in general.

- 1) The dynamics of the inner voltage controller of the inverter has been neglected and the inverter output voltages have been assumed to be equal to the references generated by the droop control strategy. This assumption is valid, as has been cited in [12] and [13], since the inner voltage controller is a fast controller with a high bandwidth, while the droop controller is a slow controller with a low bandwidth. This assumption has been made in Section II during modeling of the microgrid.
- 2) The load impedances in the microgrid will not be significantly less than 1 p.u., as smaller values would imply inverter overloads. In an inverter-based microgrid, the overload capacity is limited, as the inverters are likely to be damaged even if overloaded for short durations. However, the impedances of the interconnecting cables is much smaller in the range of 0.01–0.05 p.u., since the microgrid covers a small area. Therefore, in Section III [specifically (21)], the reciprocal of the load impedances are neglected with respect to the reciprocal of the cable impedances.
- 3) The small values of impedances of the interconnecting cables require small phase angle differences and voltage magnitude differences between inverters to produce power flow between inverters. As a result, the output voltage phasors of the inverters will be very close to each other in phase angle and magnitude. Hence, while linearizing the microgrid in Section IV, the  $d$  and  $q$  components of the inverter output voltages at the equilibrium point have been assumed to be equal. This assumption is valid for a large class of microgrids with small cable impedances.
- 4) The deviation in the voltage frequency of the microgrid is limited to 1%–2% from the nominal frequency (50–60 Hz), while deviation in voltage magnitude is limited to 2%–4% from the nominal distribution level voltage (230 or 110 V line neutral). The  $p$ - $\omega$  and  $q$ - $V$  droop control gains are therefore maintained to be small of the earlier mentioned orders. The product of two or more droop control gains will be negligible, and therefore, a term multiplied to such a product of more than one gain can be neglected. This assumption is made in the final part of the proof in Section IV.

Simulation results have been presented to show the stability of the microgrid for varying droop control gains. The boundaries of stability are obtained using Scilab. The results are very close to the results reported in literature validating the accuracy of the simplified model [11], [12]. Experimental results have been presented to show the stable operation of the microgrid.

## REFERENCES

- [1] R. Lasseter and P. Piagi, "Microgrids: A conceptual solution," in *Proc. 35th Power Electron. Spec. Conf.*, Jun. 2004, vol. 6, pp. 4285–4290.
- [2] G. Venkataramanan and M. Illindla, "Microgrids and sensitive loads," in *Proc. IEEE Power Eng. Soc. Winter Meeting*, Jan. 2001, vol. 1, pp. 315–322.
- [3] P. Loh, M. Newman, D. Zmood, and D. Holmes, "A comparative analysis of multiloop voltage regulation strategies for single and three-phase ups systems," *IEEE Trans. Power Electron.*, vol. 18, no. 5, pp. 1176–1185, Sep. 2003.
- [4] M. Chandorkar, D. Divan, and R. Adapa, "Control of parallel connected inverters in standalone ac supply systems," *IEEE Trans. Ind. Appl.*, vol. 29, no. 1, pp. 136–143, Jan./Feb. 1993.
- [5] M. Chandorkar and D. Diwan, "Decentralized operation of distributed ups systems," in *Proc. Power Electron., Drives Energy Syst. Ind. Growth*, Jan., 1996, vol. 1, pp. 565–571.
- [6] K. Brabandere, B. Bolsens, J. Keybus, A. Woyte, J. Driesen, and R. Belmans, "A voltage and frequency droop control method for parallel inverters," *IEEE Trans. Power Electron.*, vol. 22, no. 4, pp. 1107–1115, Jul. 2004.
- [7] C. Sao and P. Lehn, "Autonomous load sharing of voltage source converters," *IEEE Trans. Power Del.*, vol. 20, no. 2, pp. 1009–1016, Apr. 2005.
- [8] J. Guerrero, L. Vicuna, J. Matas, M. Castilla, and J. Miret, "Output impedance design of parallel-connected ups inverters with wireless load-sharing control," *IEEE Trans. Ind. Electron.*, vol. 52, no. 4, pp. 1126–1135, Aug. 2005.
- [9] J. Guerrero, L. Hang, and J. Uceda, "Control of distributed uninterruptible power supply systems," *IEEE Trans. Ind. Electron.*, vol. 55, no. 8, pp. 2845–2859, Aug. 2008.
- [10] E. Coelho, P. Cortizo, and P. Garcia, "Small-signal stability for parallel-connected inverters in stand-alone ac supply systems," *IEEE Trans. Ind. Appl.*, vol. 38, no. 2, pp. 533–542, Mar./Apr. 2002.
- [11] N. Pogaku, N. Prodanovic, and T. Green, "Modeling, analysis and testing of autonomous operation of an inverter-based microgrid," *IEEE Trans. Power Electron.*, vol. 22, no. 2, pp. 613–625, Mar. 2007.

- [12] E. Barklund, N. Pogaku, M. Prodanovic, C. Aramburo, and T. Green, "Energy management in autonomous microgrid using stability-constrained droop control of inverters," *IEEE Trans. Power Electron.*, vol. 23, no. 5, pp. 2346–2352, Sep. 2008.
- [13] Y. Mohamed and E. Saadany, "Adaptive decentralized droop controller to preserve power sharing stability of paralleled inverters in distributed generation microgrids," *IEEE Trans. Power Electron.*, vol. 23, no. 6, pp. 2806–2816, Nov. 2008.



**Shivkumar V. Iyer** received the B.Eng. degree in electrical engineering from Mumbai University, Mumbai, India, in 2002, and the M.Tech. degree from Indian Institute of Technology Kanpur, Kanpur, India, in 2004. He is currently working toward the Ph.D. degree in electrical engineering from Indian Institute of Technology Bombay, Mumbai.

He is currently an Associate Scientist at ABB Global Industries and Services Ltd., Bengaluru, India. His research interests include power electronics and decentralized control of modular systems.



**Madhu N. Belur** received the B.Tech. degree in mechanical engineering from Indian Institute of Technology Bombay, India, in 1997, and the Ph.D. degree in systems theory from the Institute for Mathematics and Computing Science, University of Groningen, Groningen, the Netherlands, in 2003.

Since 2003, he has been an Assistant Professor in the Department of Electrical Engineering, Indian Institute of Technology Bombay. His current research interests include works in control theory, in particular, dissipative systems, impulse-free interconnection of dynamical systems, and graph theoretic methods in control.



**Mukul C. Chandorkar** (M'84) received the B.Tech. degree from Indian Institute of Technology Bombay, Mumbai, India, the M.Tech. degree from Indian Institute of Technology, Chennai, India, and the Ph.D. degree from the University of Wisconsin, Madison, in 1984, 1987, and 1995, respectively, all in electrical engineering.

He has several years of experience in the power electronics industry in India, Europe, and the U.S. From 1996 to 1999, he was at ABB Corporate Research Ltd., Baden-Dattwil, Switzerland. He is currently a Professor in the Department of Electrical Engineering, Indian Institute of Technology Bombay, Mumbai. His research interests include uninterruptible power supplies, drives, real-time simulation of power electronic systems, and the measurement and analysis of power quality.